Draft version June 2, 2021
Typeset using LaTeX **twocolumn** style in AASTeX631

Cosmic Microwave Background map-making solutions improve with cooling

Bai-Qiang Qiang (KMH: want chinese characters?)[1] and Kevin M. Huffenberger [1]

[1] *Department of Physics, Florida State University, Tallahassee, Florida 32306*

ABSTRACT

In the context of Cosmic Microwave Background data analysis, we study the solution to the equation that transforms scanning data into a map. As originally suggested in "messenger" methods for solving linear systems, we split the noise covariance into uniform and non-uniform parts and adjusting their relative weight during the iterative solution. This "cooling" or perturbative approach is particularly effective when there is significant low-frequency noise in the timestream. A conjugate gradient algorithm applied to this modified system converges faster and to a higher fidelity solution than the standard conjugate gradient approach, for the same computational cost per iteration. We conclude that cooling is helpful separate from its appearance in the messenger methods. We give an analytical expression for the parameter that controls how gradually should change during the course of the solution.

Keywords: Computational methods — Cosmic microwave background radiation — Astronomy data reduction

1. INTRODUCTION

In observations of the Cosmic Microwave Background (CMB), map-making is an intermediate step between the collection of raw scanning data and the scientific analyses, such as the estimation of power spectra and cosmological parameters. Next generation CMB observations will generate much more data that today, and so it is worth exploring efficient ways to process the data, even though, on paper, the map-making problem has long been solved.

The time-ordered scanning data is summarized by

$$\mathbf{d} = P\mathbf{m} + \mathbf{n} \tag{1}$$

where $\mathbf{d}$, $\mathbf{m}$, and $\mathbf{n}$ are the vectors of time-ordered data (TOD), the CMB sky-map signal, and measurement noise, and P is the sparse matrix that encodes the telescope's pointing. Of several mapmaking methods (Tegmark 1997a), one of the most common is the method introduced for the Cosmic Background Explorer (COBE, Janssen & Gulkis 1992). This optimal, linear solution is

$$\left(P^\dagger N^{-1} P\right)\hat{\mathbf{m}} = P^\dagger N^{-1}\mathbf{d} \tag{2}$$

where $\hat{\mathbf{m}}$ provides the generalized least squares minimization of the χ^2 statistic

$$\chi^2(\mathbf{m}) \equiv (\mathbf{d} - P\mathbf{m})^\dagger N^{-1}(\mathbf{d} - P\mathbf{m}). \tag{3}$$

Here we assume that the noise has zero mean $\langle \mathbf{n} \rangle = \mathbf{0}$, and noise covariance matrix could be written as $N = \langle \mathbf{n}\mathbf{n}^\dagger \rangle$. We cast mapmaking as a standard linear regression problem. In case the noise is Gaussian, the COBE solution is also the maximum likelihood solution.

With current computation power, we cannot solve for $\hat{\mathbf{m}}$ by calculating $\left(P^\dagger N^{-1} P\right)^{-1} P^\dagger N^{-1}\mathbf{d}$ directly, since the $(P^\dagger N^{-1} P)$ matrix is too large to invert. The noise covariance matrix N is sparse in frequency domain and the pointing matrix P is sparse in the time-by-pixel domain, and their product is dense. In experiments currently under design, there may be $\sim 10^{16}$ time samples and $\sim 10^9$ pixels, so these matrix inversions are intractable. Therefore we use iterative methods, such as conjugate gradient descent, to avoid the matrix inversions, while executing each matrix multiplication in a basis where the matrix is sparse, using a fast Fourier transform to go between the frequency and time domain.

As an alternative technique, Huffenberger & Næss (2018) showed that the "messenger method" could be adapted to solve the linear mapmaking system, based on the approach from Elsner & Wandelt (2013) to solve the linear Wiener filter. This technique splits the noise covariance into a uniform part and the remainder, and, over the course of the iterative solution, it adjusts the relative weight of those two parts. Starting with the uniform covariance, the modified linear system gradually transforms to the final system via a cooling parameter. The cooling idea again comes from Elsner & Wan-

delt (2013). In numerical experiments, Huffenberger & Næss (2018) found that the large scales of map produced by the cooled messenger method converged significantly faster than for standard methods, and to higher fidelity.

Papež et al. (2018) showed that the iterations in the messenger field approach is equivalent to a fixed point iteration scheme, and studied its convergence properties in detail. Furthermore, they showed that the split covariance and the modified system that incorporates the cooling can be solved by other means, including a conjugate gradient technique, which should generally show better convergence properties than the fixed-point scheme. However in numerical tests, Papež et al. (2018) did not find benefits to the cooling modification of the mapmaking system, in contrast to findings of Huffenberger & Næss (2018).

In this paper, we show that the difference arose because the numerical tests in Papež et al. (2018) used much less low-frequency ($1/f$) noise than Huffenberger & Næss (2018), and show that the cooling technique improves mapmaking performance especially when the low frequency noise is large. This performance boost depends on a proper choice for the pace of cooling. Kodi Ramanah et al. (2017) showed that for Wiener filter the cooling parameter should be chosen as a geometric series. In this work, we give an alternative interpretation of the parameterizing process and show that for mapmaking the optimal choice (unsurprisingly) is also a geometric series.

In Section 2 we describe our methods for treating the mapmaking equation and our numerical experiments. In Section 3 we present our results. In Section 4 we interpret the mapmaking approach and its computational cost. In Section 5 we conclude. In appendices we derives how we set our cooling schedule.

2. METHODS

2.1. *Parameterized Conjugate Gradient Method*

The messenger field approach introduced an extra cooling parameter λ to the map-making equation, and solved the linear system with the alternative covariance $N(\lambda) = \lambda\tau I + \bar{N}$. The parameter τ represents the uniform level of (white) noise in the covariance, $\bar{N}$ is the balance of the noise, and the parameterized covariance equals the original covariance when the cooling parameter $\lambda = 1$. In this work we find it more convenient to work with the inverse cooling parameter $\eta = \lambda^{-1}$ and define the covariance as

$$N(\eta) = \tau I + \eta\bar{N} \tag{4}$$

which leads to the same system of mapmaking equations. (This is because $N(\eta) = \lambda^{-1}N(\lambda)$ and the mapmaking equation is insensitive to to scalar multiple of the covariance since is appears on both sides.)

Papež et al. (2018) showed that the conjugate gradient method can be easily applied to parameterized mapmaking equation by iterating on

$$P^\dagger N(\eta)^{-1}P\ \hat{\mathbf{m}} = P^\dagger N(\eta)^{-1}\mathbf{d} \tag{5}$$

as the cooling is adjusted. In our numerical experiments, we confirm that the conjugate gradient approach is converging faster than the fixed point iterations suggested by the messenger mapmaking method in Huffenberger & Næss (2018). For simplicity we fix the preconditioner to $M = P^\dagger P$ for all of calculations.

When $\eta = 0$, the noise covariance matrix $N(0)$ is proportional to identity matrix I, and solution is given by simple binned map $\mathbf{m}_0 = \left(P^\dagger P\right)^{-1}P^\dagger\mathbf{d}$, which can be solved directly. From this starting point, the cooling scheme requires the inverse cooling parameter η increase as $0 = \eta_0 \le \eta_1 \le \cdots \le \eta_{\rm final} = 1$, at which point we arrive at the desired mapmaking equation. For each intermediate η_i, we treat it as a seperate conjugate gradient method to solve equation $\left(P^\dagger N(\eta_i)^{-1}P\right)\hat{\mathbf{m}}(\eta_i) = P^\dagger N(\eta_i)^{-1}\mathbf{d}$, using the result from previous calculation $\hat{\mathbf{m}}(\eta_{i-1})$ as the initial value, and move to next parameter η_{i+1} when $\left(P^\dagger N(\eta_i)^{-1}P\right)\hat{\mathbf{m}}(\eta_i) - P^\dagger N(\eta_i)^{-1}\mathbf{d} \simeq 0$, KMH: In this description, it is not totally clear whether you intend to update the eta after every iteration.

The non-white part $\bar{N}$ is the troublesome portion of the covariance, and we can think of the η parameter as turning it on slowly, adding a perturbation to the solution achieved at a particular stage, building ultimately upon the initial uniform covariance model.

2.2. *Choice of inverse cooling parameters η*

The next question is how we choose these monotonically increasing parameters η. If we choose them inappropriately, the solution converge slowly, because we waste effort converging on the wrong system. We also want to determine $\eta_1, \cdots, \eta_{n-1}$ before starting conjugate gradient iterations. The time ordered data $\mathbf{d}$ is very large, and we do not want to keep it in the system memory during calculation. If we determine $\eta_1, \cdots, \eta_{n-1}$ before the iterations, then we can precompute the right-hand side $P^\dagger N(\eta)^{-1}\mathbf{d}$ for each η_i and keep these map-sized objects in memory, instead of the entire time-ordered data.

In the appendix, we show that a generic good choice for the η parameters are the geometric series

$$\eta_i = \min\left\{\left(2^i - 1\right)\frac{\tau}{\max(\bar{N}_f)},\ 1\right\}, \tag{6}$$

where $\bar{N}_f$ is the frequency representation of the non-uniform part of the covariance. This is the main result.

It tells us not only how to choose parameters η_i, but also when we should stop the perturbation, and set $\eta = 1$. For example, if noise covariance matrix N is almost white noise, then $\bar{N} = N - \tau I \approx 0$, and we would have $\tau/\max(\bar{N}_f) \gg 1$. This tell us that we don't need to use parameterized method at all, because $\eta_0 = 0$ and $\eta_1 = \eta_2 = \cdots = 1$. This corresponds to the standard conjugate gradient method with simple binned map as the initial guess (as recommended by Papež et al. 2018).

2.3. *Numerical Simulations*

To compare these algorithms, we need to do some simple simulation of scanning processes, and generate time ordered data from random sky signal.[1] Our sky is a small rectangular area, with two orthogonal directions x and y, both with range from $-1°$ to $+1°$. The signal has first three stokes parameters (I, Q, U).

For the scanning process, our single telescope contains nine detectors, each has different sensitivity to polarization Q and U. It scans the sky with a raster scanning pattern and scanning frequency $f_{\rm scan} = 0.1$ Hz sampling frequency $f_{\rm sample} = 100$ Hz. The telescope scans the sky horizontally and then vertically, and then digitizes the position (x, y) into 512×512 pixel. This gives noiseless signal $\mathbf{s}$.

The noise power spectrum is given by

$$P(f) = \sigma^2 \left(1 + \frac{f_{\rm knee}^\alpha + f_{\rm apo}^\alpha}{f^\alpha + f_{\rm apo}^\alpha}\right) \tag{7}$$

Here we fixed $\sigma^2 = 10\ \mu\mathrm{K}^2$, $\alpha = 2$ and $f_{\rm knee} = 10$ Hz, and change $f_{\rm apo}$ to compare the performance under different noise models. Note that as $f_{\rm apo} \to 0$, $P(f) \to \sigma^2\left(1 + (f/f_{\rm knee})^{-1}\right)$, it becomes a $1/f$ noise model. The noise covariance matrix

$$N_{ff'} = P(f)\frac{\delta_{ff'}}{\Delta_f} \tag{8}$$

is a diagonal matrix in frequency space, where Δ_f is equal to reciprocal of total scanning time T. In our calculations we choose the $f_{\rm apo}$ such that the condition numbers κ are 10^2, 10^6, and 10^{12}. The corresponding power spectrum are shown in Figure(1).

Finally, we get the simulated time ordered data $\mathbf{d} = \mathbf{s} + \mathbf{n}$ by adding up signal and noise.

KMH: Compare to the noise power spectrum of Papez. Remark how little 1/f is in their test. What is the effect of changing the noise slope? In Papež et al. 2018, the noise power spectrum is apodized at $0.1 f_{\rm knee}$, which corresponds to $f_{\rm apo} \approx 0.1 f_{\rm knee}$ For the case $f_{\rm knee} = 10$ and $\kappa = 100$, the apodization frequency $f_{\rm apo} \approx 0.99 \approx 0.1 f_{\rm knee}$. Therefore the blue line in Figure (1), is close to the power spectrum used in Papež et al. 2018.

[1] The source code and other information are available at https://github.com/Bai-Qiang/map_making_perturbative_approach

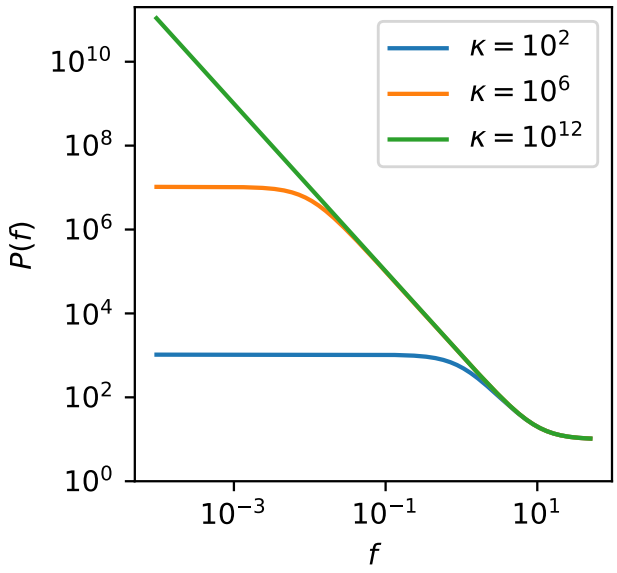

Figure 1. The noise power spectum based on Eq. (7) with $\sigma^2 = 10\ \mu\mathrm{K}^2$, $\alpha = 2$ and $f_{\rm knee} = 10$ Hz. And fixing the condition number κ of noise covariance matrix Eq. (8) by choosing $f_{\rm apo}$. KMH: show the scanning freqency with a vertical (dashed?) line. Can use axvline().

3. RESULTS

First let's compare the results with vanilla conjugate gradient method with simple preconditioner $P^\dagger P$. The results are showed in Figure (2) for different kinds of noise power spectra. Here note that χ^2 in all figures are calculated based on Eq. (3) not $\chi^2(\mathbf{m}, \eta)$ in Eq. (**??**). The $\chi^2_{\rm min}$ is calculated from perturbative conjugate gradient method with more intermediate η values, and more iterations after $\eta = 1$.

As we can see in the left graph in Figure(2), when the condition number of noise covariance matrix $\kappa(N)$ is small, the performance between different these two methods are small. The vanilla conjugate gradient method converge faster, because its perturbation parameter goes to 1 at the first iteration, however for the perturbation method its η value will slowly reach 1 in about ten iterations.

Notice that as we increase $\kappa(N)$, or equivalently decrease $f_{\rm apo}$, the perturbation parameter η starts showing its benefits, as showed in the second and third graph in Figure(2). It outperforms the vanilla conjugate gradient method when $f_{\rm apo} \approx 0$ and the noise power spectrum be-

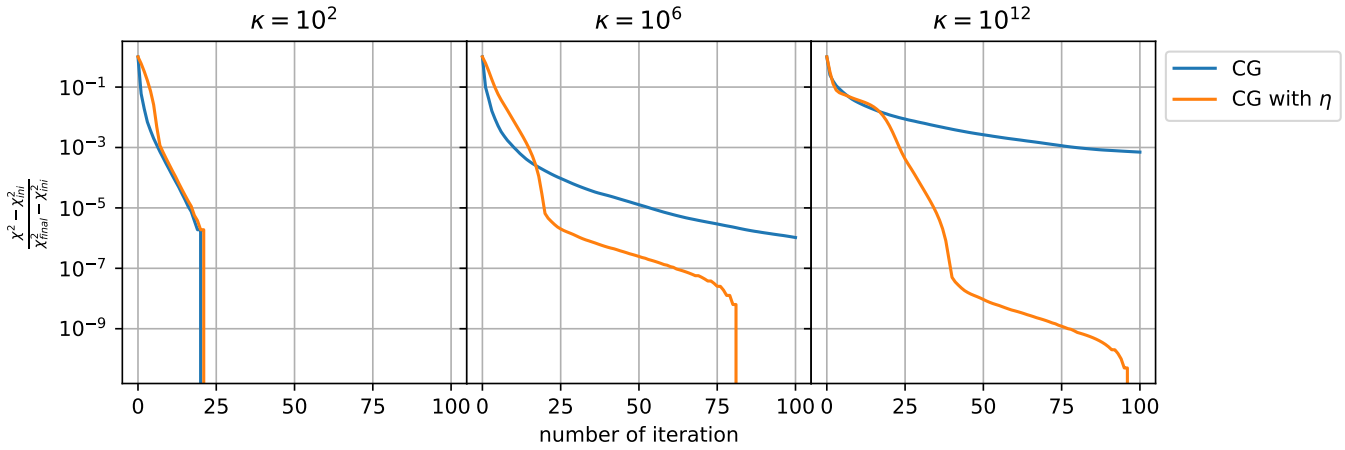

Figure 2. These three figures show the $\frac{\chi^2(\mathbf{m})-\chi^2_{\rm ini}}{\chi^2_{\rm min}-\chi^2_{\rm ini}}$ changes for each iteration under different noise covariance matrix with condition number being 10^2, 10^6, and 10^{12}.

comes the $1/f$ noise model, which usually is the intrinsic noise of instruments (Tegmark (1997b)).

Now let us compare the performance difference between choosing η parameters based on Eq. (6) and manually fixing number of η parameters n_η manually. We manually choose the η_i values using function `numpy.logspace(start=`$\ln(\eta_1)$`, stop=0, num=`n_η`, base=`e`)`. The results are showed in Figure(3).

When $\kappa(N)$ is small, and Eq. (6) tells us that only a few η parameters are good enough, see the orange line in the first Figure(3), where we have ~ 10 η levels. If unfortunately we choose n_η being large value, like 15 or 30, then it will ends up converge slowly, because it needs at least 15 or 30 iterations to reach $\eta = 1$, at least one iteration per η level.

On the other hand if $\kappa(N)$ is very large and the power spectrum is $1/f$ noise, we need more η parameters. If n_η is too small, for example $n_\eta = 5$ the green line in last Figure(3), it may be better than the vanilla conjugate gradient method, but it is still far from optimal.

Since the η values determined from Eq. (6)

$$\eta_i = \min\left\{1,\ \frac{\tau}{\max(\bar{N}_f)}\left(2^i - 1\right)\right\} \tag{6}$$

are not dependent on any scanning information, it only depends on noise power spectrum $P(f)$, or noise covariance matrix N. Figure (**??**) and Figure (**??**) show two examples with same parameters as in Figure (3) except for the scanning frequency $f_{\rm scan}$ in Figure (**??**) it scans very slow and in Figure (**??**) it's very fast. In these two cases under $1/f$ noise model, our η values based on Eq. (6) are better than manually selected values. Based on these two results we know, the η values should somehow depends on scanning scheme.

4. DISCUSSION

4.1. *Intuitive Interpretation of η*

KMH: most of this is pretty similar to discussion in Huffenberger and Naess. The last paragraph is new.

In this section, let me introduce another way to understand the role of η. Our ultimate goal is to find $\hat{\mathbf{m}}(\eta = 1)$ which minimizes $\chi^2(\mathbf{m}) = (\mathbf{d} - P\mathbf{m})^\dagger N^{-1}(\mathbf{d} - P\mathbf{m})$. Since N is diagonal in frequency space, χ^2 could be written as a sum of all frequency mode $|(\mathbf{d} - P\mathbf{m})_f|^2$ with weight N_f^{-1}, such as $\chi^2(\mathbf{m}) = \sum_f |(\mathbf{d} - P\mathbf{m})_f|^2 N_f^{-1}$. N_f^{-1} is large when there is little noise at that frequency, and vice versa. Which means $\chi^2(\mathbf{m})$ would favor the low noise frequency mode over high noise ones. In other words the optimal map $\hat{\mathbf{m}}$ focusing on minimize the error $\mathbf{r} \equiv \mathbf{d} - P\mathbf{m}$ in the low-noise part.

After introducing η, we minimize $\chi^2(\mathbf{m}, \eta) = (\mathbf{d} - P\mathbf{m})^\dagger N_\eta^{-1}(\mathbf{d} - P\mathbf{m})$. For $\eta = 0$, $N^{-1}_{\eta=0} \propto I$ and the estimated map $\hat{\mathbf{m}}(\eta = 0)$ does not prioritize any frequency mode. As we slowly increase η, we decrease the weight for the frequency modes which have large noise, and focusing minimizing error for low noise part. If we start with $\eta_1 = 1$ directly, which corresponds to the vanilla conjugate gradient method, then the entire conjugate gradient solver will focus most on minimizing the low noise part, such that χ^2 would converge very fast at low noise region, but slowly on high noise part. Since it focus on low noise part only, it may be stuck at some local minimum point. To get to the global minimum, it need to adjust the low noise part, that would be difficult if it's stuck at an local minimum. However by introducing η parameter, we let the solver first treat every frequency equally. Then as η slowly increases, it gradually shifts focus from the highest noise to the lowest noise part. KMH: I feel what this is missing is why the high-noise modes get stuck though.

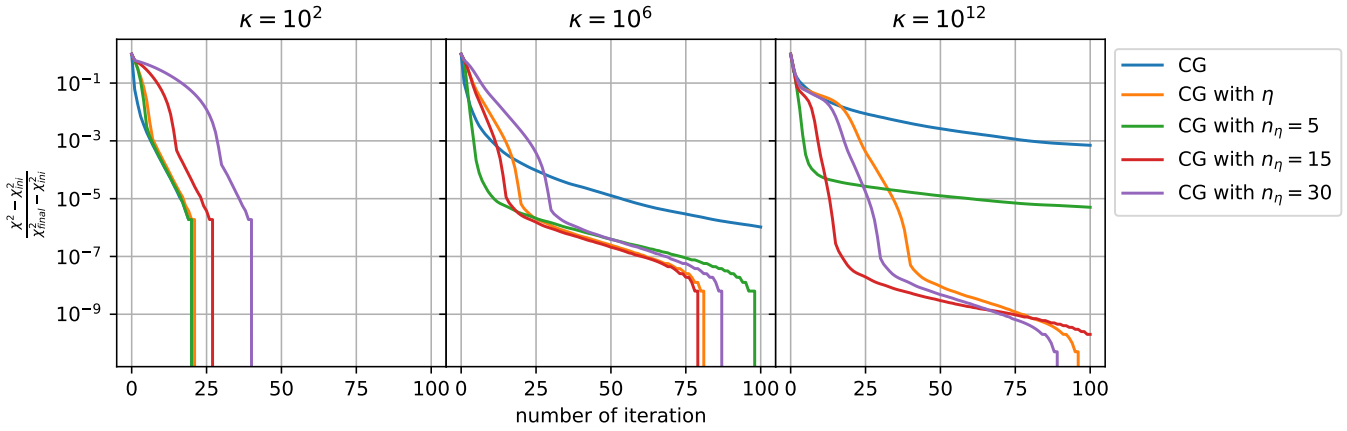

Figure 3. The blue line and the orange line are the same as Figure (2). For three extra lines, we fix the number of η parameter n_η manully. Instead of using Eq. (6), we use `numpy.logspace(start=`$\ln(\eta_1)$`, stop=0, num=`n_η`, base=`e`)`. to get all η parameters.

If we write the difference between final and initial χ^2 value as $\chi^2(\hat{\mathbf{m}}(1), 1) - \chi^2(\hat{\mathbf{m}}(0), 0) = \int_0^1 \mathrm{d}\eta \frac{\mathrm{d}}{\mathrm{d}\eta}\chi^2(\hat{\mathbf{m}}(\eta), \eta)$, and use Eq. (A2). We note that when η is very small, the $\frac{\mathrm{d}}{\mathrm{d}\eta}\chi^2(\hat{\mathbf{m}}(\eta), \eta)$ would have relatively large contribution from medium to large noise region, comparing to large η. So introducing η might improve the convergence of χ^2 at these regions, because the vanilla conjugate gradient method only focuses on the low noise part and it may have difficulty at these regions.

4.2. *Computational Cost*

To properly compare the performance cost of this method with respect to vanilla conjugate gradient method with simple preconditioner, we need to compare their computational cost at each iteration. The right hand side of parameterized map-making equation Eq. (5) could be computed before iterations, so it won't introduce extra computational cost. The most demanding part of conjugate gradient method is calculating $P^\dagger N^{-1} P\hat{\mathbf{m}}$, because it contains a Fourier transform of $P\hat{\mathbf{m}}$ from time domain to frequency domain and an inverse Fourier transform of $N^{-1}P\hat{\mathbf{m}}$ from frequency domain back to time domain, which is order $\mathcal{O}(n \log n)$ with n being the length of time ordered data. If we change N^{-1} to $N(\eta)^{-1}$, it won't add extra cost, since both matrices are diagonal in frequency domain. Therefore the computational cost it the same for one step.

However our previous analysis is based on $\chi^2(\hat{\mathbf{m}}(\eta_i), \eta_i)$ which is evaluated at $\hat{\mathbf{m}}(\eta_i)$ the estimated map at η_i. So We should update η_i to η_{i+1} when $\mathbf{m} \approx \hat{\mathbf{m}}(\eta_i)$. How do we know this condition is satisfied? Since for each new η_i value, we are solving a new set of linear equations $A(\eta_i)\hat{\mathbf{m}} = \mathbf{b}(\eta_i)$ with $A(\eta_i) = P^\dagger N(\eta_i)^{-1} P$ and $\mathbf{b}(\eta_i) = P^\dagger N(\eta_i)^{-1}\mathbf{d}$, and we could stop calculation and moving to next value η_{i+1} when the norm of residual $||\mathbf{r}(\eta_i)|| = ||\mathbf{b}(\eta_i) - A(\eta_i)\mathbf{m}||$ smaller than some small value. Calculate $||\mathbf{r}(\eta_i)||$ is part of conjugate gradient algorithm, so this won't add extra cost compare to vanilla conjugate gradient method. Therefore, overall introducing η won't have extra computational cost.

4.3. *Future Prospects*

KMH: some of this future prospects should move to discussion As you may have noticed in the second and third Figure(3), the perturbation parameter based on Eq. (6) is more than needed, especially for $1/f$ noise case. For the case $\kappa = 10^{12}$, we notice that based on Eq. (6) it gives us $n_\eta \approx 40$, however from χ^2 result in the last Figure(3) $n_\eta \approx 30$ or even $n_\eta \approx 15$ is good enough. Also, for the nearly-white-noise case, we could certainly choose $n_\eta = 1$ such that $\eta_1 = 1$ which corresponds to vanilla conjugate gradient method, based on χ^2 result in first Figure(3). However Eq. (6) gives us $n_\eta \approx 6$, even though it does not make the final χ^2 result much different at the end.

Is it possible to further improve the analysis, such that it produces smaller n_η? Let's examine how we get η_i series. Remember that we determine $\delta\eta$ value based on the upper bound of $-\delta\chi^2(\hat{\mathbf{m}}(\eta), \eta)/\chi^2(\hat{\mathbf{m}}(\eta), \eta)$, in Eq. (**??**). For $\eta \neq 0$, the upper bound is

$$\delta\eta \frac{\hat{\mathbf{r}}_\eta^\dagger N(\eta)^{-1}\bar{N}N(\eta)^{-1}\hat{\mathbf{r}}_\eta}{\hat{\mathbf{r}}_\eta^\dagger N(\eta)^{-1}\hat{\mathbf{r}}_\eta} \leq \frac{\delta\eta}{\eta + \frac{\tau}{\max(N_f) - \tau}} \tag{9}$$

with $\mathbf{r}_\eta = \left[1 - P\left(P^\dagger N(\eta)^{-1} P\right)^{-1} P^\dagger N(\eta)^{-1}\right]\mathbf{d} \equiv \mathcal{P}_\eta \mathbf{d}$. To get the upper bound we treated $\mathbf{d} - P\hat{\mathbf{m}}(\eta)$ as an arbitrary vector in frequency domain, since we don't know how to calculate $\mathcal{P}_\eta$ for $\eta \neq 0$, and it's hard to analyze

the projection matrix $\mathcal{P}_\eta$ in frequency space, as it contains $\left(P^\dagger N(\eta)^{-1}P\right)^{-1}$. Note that we have to determine all of η value before calculation, because we don't want to keep the time ordered data in system RAM, so we need to somehow analytically analyze $\mathcal{P}_\eta$, and its behavior in frequency space. Unless $\mathbf{r}_\eta$ almost only has large noise modes, $\left|\frac{\mathrm{d}}{\mathrm{d}\eta}\chi^2(\hat{\mathbf{m}}(\eta),\eta)/\chi^2(\hat{\mathbf{m}}(\eta),\eta)\right|$ won't get close to the upper bound $1/\left(\eta+\frac{\tau}{\max(N_f)-\tau}\right)$. Based on the analysis in Section(4.1), for small η the estimated map $\hat{\mathbf{m}}(\eta)$ does not only focusing on minimizing error $\mathbf{r}_\eta$ at low noise region. So we would expect that there would be a fair amount of low noise modes contribution in $\mathbf{r}_\eta$ especially for the first few η values. Which means if we could somehow know the frequency distribution of $\mathbf{r}_\eta$, we could tighten the boundary of $\left|\frac{\mathrm{d}}{\mathrm{d}\eta}\chi^2(\hat{\mathbf{m}}(\eta),\eta)/\chi^2(\hat{\mathbf{m}}(\eta),\eta)\right|$, and get larger $\delta\eta$ value. This should make η goes to 1 faster, and yields the fewer η parameters we need.

Also notice that the η values determined from Eq. (6) are not dependent on any scanning information, it only depends on noise power spectrum $P(f)$, or noise covariance matrix N. In Appendix **??** we would show two examples with same parameters as in Figure(3) except scanning frequency f_{scan}.It turns out the η values should somehow depends on scanning scheme. Again that's because when we determine the upper boundwe treated $\mathbf{r}_\eta$ as an arbitrary vector, such that we lose all information related to scanning scheme in the pointing matrix P.

5. CONCLUSIONS

KMH: We need some discussion of the things that haven't yet been demonstrated with the PCG, like multiple messenger fields. Has the Kodi-Ramanah dual messenger field scheme been demonstrated in a PCG scheme by Papez?

Even though the perturbation parameter η get from Eq. (6) are not the most optimal, it still performs much better than traditional conjugate gradient method under $1/f$ noise scenario without adding extra computational cost. The only extra free parameter added is to determine whether the error at current step $\mathbf{r}(\eta_i) = ||\mathbf{b}(\eta_i) - A(\eta_i)\mathbf{m}||$ is small enough such that we advance to next value η_{i+1}.

Also this analysis of η value also explains why cooling parameters $\lambda = 1/\eta$ in messenger field are chosen to be geometric series or `logspace` used in Huffenberger & Næss (2018).

All of the calculation are using simple preconditioner $P^\dagger P$, but the entire analysis is independent of preconditioner. Better preconditioners would also lead to improvements.

BQ and KH are supported by NSF award 1815887.

APPENDIX

A. THE SEQUENCE OF INVERSE COOLING PARAMETERS

We know that the initial inverse cooling parameter $\eta_0 = 0$. What would be good value for the next parameter η_1? To simplify notation, we use N_η to denote $N(\eta) = \tau I + \eta\bar{N}$. For some specific η value, the minimum χ^2 value is given by the optimized map $\hat{\mathbf{m}}(\eta) = \left(P^\dagger N_\eta^{-1}P\right)^{-1}P^\dagger N_\eta^{-1}\mathbf{d}$, which minimizes

$$\chi^2(\hat{\mathbf{m}}(\eta),\eta) = \left(\mathbf{d} - P\hat{\mathbf{m}}(\eta)\right)^\dagger N_\eta^{-1}\left(\mathbf{d} - P\hat{\mathbf{m}}(\eta)\right). \tag{A1}$$

We restrict to the case that the noise covariance matrix N is diagonal in the frequency domain, and represent the frequency-domain eigenvalues as N_f.

Let us first consider $\eta_1 = \eta_0 + \delta\eta = \delta\eta$ such that $\eta_1 = \delta\eta$ is very small quantity, $\delta\eta \ll 1$. Since $\hat{\mathbf{m}}(\eta)$ minimizes $\chi^2(\hat{\mathbf{m}}(\eta),\eta)$, we have $\frac{\partial}{\partial\hat{\mathbf{m}}}\chi^2(\hat{\mathbf{m}}(\eta),\eta) = 0$, and using chain rule

$$\frac{\mathrm{d}}{\mathrm{d}\eta}\chi^2(\hat{\mathbf{m}}(\eta),\eta) = \frac{\partial}{\partial\eta}\chi^2(\hat{\mathbf{m}}(\eta),\eta) = -(\mathbf{d} - P\hat{\mathbf{m}}(\eta))^\dagger N_\eta^{-1}\bar{N}N_\eta^{-1}(\mathbf{d} - P\hat{\mathbf{m}}(\eta)) \tag{A2}$$

Then the fractional decrease of $\chi^2(\hat{\mathbf{m}}(0),0)$ from $\eta_0 = 0$ to $\eta_1 = \delta\eta$ is

$$-\frac{\delta\chi^2(\hat{\mathbf{m}}(0),0)}{\chi^2(\hat{\mathbf{m}}(0),0)} = -\delta\eta\frac{\frac{\mathrm{d}}{\mathrm{d}\eta}\chi^2(\hat{\mathbf{m}}(0),0)}{\chi^2(\hat{\mathbf{m}}(0),0)} = \delta\eta\frac{1}{\tau}\frac{(\mathbf{d} - P\hat{\mathbf{m}}(0))^\dagger\bar{N}(\mathbf{d} - P\hat{\mathbf{m}}(0))}{\left(\mathbf{d} - P\hat{\mathbf{m}}(0)\right)^\dagger\left(\mathbf{d} - P\hat{\mathbf{m}}(0)\right)} \tag{A3}$$

Here we put a minus sign in front of this expression such that it's non-negative, and use $N_{\eta=0} = \tau I$ at the second equality. Since it is hard to analyze $\mathbf{d} - P\hat{\mathbf{m}}$ under frequency domain, we treat it as an arbitary vector, then the least

upper bound is given by

$$-\frac{\delta\chi^2(\hat{\mathbf{m}}(0),0)}{\chi^2(\hat{\mathbf{m}}(0),0)} \leq \frac{\delta\eta}{\tau}\max(\bar{N}_f) \tag{A4}$$

where $\max(\bar{N}_f)$ is the maxium eigenvalue of $\bar{N}$. Here if we assume that initial χ^2 value $\chi^2(\hat{\mathbf{m}}(0),0)$ is much larger than final value $\chi^2(\hat{\mathbf{m}}(1),1)$, $\chi^2(\hat{\mathbf{m}}(0),0) \gg \chi^2(\hat{\mathbf{m}}(1),1)$, then we would expect

$$-\frac{\delta\chi^2(\hat{\mathbf{m}}(0),0)}{\chi^2(\hat{\mathbf{m}}(0),0)} = 1 - \frac{\chi^2(\hat{\mathbf{m}}(1),1)}{\chi^2(\hat{\mathbf{m}}(0),0)} \approx 1^- \tag{A5}$$

The upper bound is strictly smaller than 1. Ideally, if $\delta\chi^2(\hat{\mathbf{m}}(0),0) = \chi^2(\hat{\mathbf{m}}(1),1) - \chi^2(\hat{\mathbf{m}}(0),0)$, then it would get close to the final χ^2 at next iteration, but we do not know the final $\chi^2(\hat{\mathbf{m}}(1),1)$. So we want $\left|\frac{\delta\chi^2(\hat{\mathbf{m}}(0),0)}{\chi^2(\hat{\mathbf{m}}(0),0)}\right|$ to be as large as possible, so it could converge fast, but subject to another constraint that the least upper bound cannot exceed 1. Therefore we can choose $\delta\eta$ such that the least upper bound is equal to 1. Thus we choose

$$\eta_1 \equiv \frac{\tau}{\max(\bar{N}_f)} = \frac{\min(N_f)}{\max(N_f) - \min(N_f)}. \tag{A6}$$

Here N_f and $\bar{N}_f$ are the eigenvalues of N and $\bar{N}$ in the frequency domain. If the condition number of noise covariance matrix $\kappa(N) = \max(N_f)/\min(N_f) \gg 1$, then $\eta_1 \approx \kappa^{-1}(N)$.

What about the other parameters η_m with $m > 1$? We use a similar analysis, letting $\eta_{m+1} = \eta_m + \delta\eta_m$ with a small $\delta\eta_m \ll 1$, and set the least upper bound of relative decrease equal to 1.

$$\begin{aligned}
-\frac{\delta\chi^2(\hat{\mathbf{m}}(\eta_m),\eta_m)}{\chi^2(\hat{\mathbf{m}}(\eta_m),\eta_m)} =& \delta\eta_m \frac{(\mathbf{d} - P\hat{\mathbf{m}}(\eta_m))^\dagger N_{\eta_m}^{-1}\bar{N}N_{\eta_m}^{-1}(\mathbf{d} - P\hat{\mathbf{m}}(\eta_m))}{\big(\mathbf{d} - P\hat{\mathbf{m}}(\eta_m)\big)^\dagger N_{\eta_m}^{-1}\big(\mathbf{d} - P\hat{\mathbf{m}}(\eta_m)\big)} \\
\leq& \delta\eta_m \max\left(\frac{\bar{N}_f}{\tau + \eta_m\bar{N}_f}\right)
\end{aligned} \tag{A7}$$

The upper bound in the second line is a little bit tricky. Both matrix $\bar{N}$ and $N_{\eta_m}^{-1}$ can be simultaneously diagonalized in frequency space. For each eigenvector $\mathbf{e}_f$, the corresponding eigenvalue of the matrix on the numerator $N_{\eta_m}^{-1}\bar{N}N_{\eta_m}^{-1}$ is $\lambda_f = \bar{N}_f(\tau + \eta_m\bar{N}_f)^{-2}$, and the eigenvalue for matrix on the denominator $N_{\eta_m}^{-1}$ is $\gamma_f = (\tau + \eta_m\bar{N}_f)^{-1}$. Their eigenvalues are related by $\lambda_f = [\bar{N}_f/(\tau + \eta_m\bar{N}_f)]\gamma_f$. For any vector $\mathbf{v} = \sum_f \alpha_f\mathbf{e}_f$, we have

$$\frac{\mathbf{v}^\dagger N_{\eta_m}^{-1}\bar{N}N_{\eta_m}^{-1}\mathbf{v}}{\mathbf{v}^\dagger N_{\eta_m}^{-1}\mathbf{v}} = \frac{\sum_f \alpha_f^2\lambda_f}{\sum_f \alpha_f^2\gamma_f} = \frac{\sum_f \alpha_f^2\gamma_f\bar{N}_f/(\tau + \eta_m\bar{N}_f)}{\sum_f \alpha_f^2\gamma_f} \leq \max\left(\frac{\bar{N}_f}{\tau + \eta_m\bar{N}_f}\right). \tag{A8}$$

Similarly, we could set the least upper bound equal to 1. Then we get

$$\delta\eta_m = \min\left(\frac{\tau + \eta_m\bar{N}_f}{\bar{N}_f}\right) = \eta_m + \frac{\tau}{\max(\bar{N}_f)}. \tag{A9}$$

Therefore

$$\eta_{m+1} = \eta_m + \delta\eta_m = 2\eta_m + \frac{\tau}{\max(\bar{N}_f)} \tag{A10}$$

The final term $\tau/\max(\bar{N}_f) = \eta_1$ becomes subdominant after a few terms, and we see that the η_m increase like a geometric series. Here we assumed that $\chi^2(\hat{\mathbf{m}}(\eta_m),\eta_m) \gg \chi^2(\hat{\mathbf{m}}(1),1)$, which we expect it to be satisfied for our assumed $\eta_m \ll 1$. Since the final result is geometric series, only the last few η_m values fail to be much smaller than 1.

If written in the form $\eta_{m+1} + \tau/\max(\bar{N}_f) = 2\big(\eta_m + \tau/\max(\bar{N}_f)\big)$ it's easy to see that for $m \geq 1$, $\eta_m + \tau/\max(\bar{N}_f)$ forms a geometric series

$$\eta_m + \frac{\tau}{\max(\bar{N}_f)} = \left(\eta_1 + \frac{\tau}{\max(\bar{N}_f)}\right)2^{m-1} = \frac{\tau}{\max(\bar{N}_f)}2^m \tag{A11}$$

where we used $\eta_1 = \tau/\max(\bar{N}_f)$. Note that $m = 0$ and $\eta_0 = 0$ also satisfy this expression and we've got final expression for all η_m

$$\eta_m = \min\left\{1,\ \frac{\tau}{\max(\bar{N}_f)}(2^m - 1)\right\} \tag{A12}$$

Here we need to truncate the series when $\eta_m > 1$.

REFERENCES

Elsner, F., & Wandelt, B. D. 2013, A&A, 549, A111, doi: 10.1051/0004-6361/201220586

Huffenberger, K. M., & Næss, S. K. 2018, The Astrophysical Journal, 852, 92, doi: 10.3847/1538-4357/aa9c7d

Janssen, M. A., & Gulkis, S. 1992, in NATO Advanced Science Institutes (ASI) Series C, ed. M. Signore & C. Dupraz, Vol. 359 (Springer), 391–408

Kodi Ramanah, D., Lavaux, G., & Wandelt, B. D. 2017, MNRAS, 468, 1782, doi: 10.1093/mnras/stx527

Papež, J., Grigori, L., & Stompor, R. 2018, A&A, 620, A59, doi: 10.1051/0004-6361/201832987

Tegmark, M. 1997a, ApJL, 480, L87, doi: 10.1086/310631

—. 1997b, PhRvD, 56, 4514, doi: 10.1103/PhysRevD.56.4514